



Cite this: *Nanoscale*, 2014, 6, 14343

In vivo multimodality imaging of miRNA-16 iron nanoparticle reversing drug resistance to chemotherapy in a mouse gastric cancer model†

Zhongchan Sun,^{‡a,b} Xinxing Song,^{‡b,c} Xiujuan Li,^b Tao Su,^b Shun Qi,^d Ruirui Qiao,^e Fu Wang,^f Yi Huan,^d Weidong Yang,^g Jing Wang,^g Yongzhan Nie,^h Kaichun Wu,^h Mingyuan Gao^e and Feng Cao^{*a,b}

miRNA-16 (miR16) plays an important role in modulating the drug resistance of SGC7901 cell lines to adriamycin (ADR). A variety of viral carriers have been designed for miRNA delivery. However, the safety concerns are currently perceived as hampering the clinical application of viral vector-based therapy. Herein a type of magnetic nanoparticles (MNPs) was designed and synthesized using poly(ethylene glycol) (PEG)-coated Fe₃O₄ nanoparticles as a miRNA delivery system for the purpose of reducing drug resistance of gastric cancer cells by enforcing miR16 expression in SGC7901/ADR cells. The MNPs with good biocompatibility were synthesized by thermal decomposition, and then conjugated with miRNA *via* electrostatic interaction producing miR16/MNPs. After co-culture with miR16/MNPs, ADR-induced apoptosis of SGC7901/ADR was examined by MTT and TUNEL. miR16/MNPs treatment significantly increased cell apoptosis *in vitro*. SGC7901/ADR^{fluc} tumor-bearing nude mice under ADR therapy were treated with miR16/MNPs by tail vein injection for *in vivo* study. After intraperitoneal injection of ADR, tumor volume measurement and fluorescence imaging were performed to for the death of SGC7901/ADR cells *in vivo*. Results showed that miR16/MNPs were able to significantly suppress SGC7901/ADR tumor growth, probably through increasing SGC7901/ADR cells' sensitivity to ADR. Our results suggest the efficient delivery of miR16 by MNPs as a novel therapeutic strategy for drug resistant tumor treatment.

Received 13th August 2014,
Accepted 29th September 2014

DOI: 10.1039/c4nr03003f

www.rsc.org/nanoscale

Introduction

Gastric cancer is one of the most common human malignancies and the second leading cause of cancer death in the world.¹ It is generally accepted that drug resistance is a major

contributor to chemotherapy failure for gastric cancer.² Therefore, reversing drug resistance is a novel strategy for drug resistant tumor treatment and may enhance the effectiveness of chemotherapy.

microRNAs (miRNAs) are a well-known class of small RNAs that inhibit gene expression at the post-transcriptional level by directly targeting the regions of sequence complementarity in the 3'-untranslated regions (3'-UTRs) of mRNAs. The manipulation of miRNA is considered as a novel strategy for reversing drug resistance in tumor cells.³ miRNA-16 (miR16) is a well-recognized tumor-suppressing miRNA^{4,5} and our previous work showed miR16 was able to sensitize drug resistant gastric cancer cells by down-regulating its target protein Bcl-2, an anti-apoptotic gene, which was found to be elevated in drug resistant cells.⁶ Theoretically, exogenous delivery of miR16 would sensitize drug resistant gastric cancer cells and significantly enhance the therapeutic effect of anti-tumor medication. A variety of viral carriers have been designed for miRNA delivery and have shown high transfection efficiencies over a broad range of cell types. However, the safety concerns are currently perceived as hampering the clinical application of viral vector-based therapy.

^aDepartment of Cardiology, Chinese PLA General Hospital, Beijing, 100853, China.
E-mail: wind8828@gmail.com; Fax: +86-29-84775183; Tel: +86-29-84771024

^bDepartment of Cardiology, Xijing Hospital, Fourth Military Medical University, Xi'an 710032, China

^cDepartment of Cardiology, 285 Hospital, Handan 056001, China

^dDepartment of Radiology, Xijing Hospital, Fourth Military Medical University, Xi'an 710032, China

^eInstitute of Chemistry, Chinese Academy of Sciences, Bei Yi Jie 2, Zhong Guan Cun, Beijing 100190, China

^fLife Sciences Research Center, School of Life Sciences and Technology, Xidian University, Xi'an 710071, China

^gDepartment of Nuclear Medicine, Xijing Hospital, Fourth Military Medical University, Xi'an 710032, China

^hDepartment of Digestive Disease, Xijing Hospital, Fourth Military Medical University, Xi'an 710032, China

† Electronic supplementary information (ESI) available. See DOI: 10.1039/c4nr03003f

‡ These authors contributed equally to this work and should be considered as co-first authors

Nanoparticles are developed as a delivery platform for molecules and reagents used in human cancer diagnosis and therapy by taking advantage of their unique physicochemical property.^{7–9} Because of their appropriate diameters and the enhanced permeability of tumor vasculature, nanoparticles can accumulate passively in tumors by enhanced permeability and retention (EPR) effect.¹⁰ Recently, accumulating evidence also suggested that nanoparticles can function as a good delivery system for miRNA.^{11–13} Moreover, nanoparticles are able to be dynamically traced by MRI, ultrasound, and optical imaging *in vivo* owing to their own physical performance or through conjugation with various specific labeling markers. This particular property of nanoparticles noninvasively allows the determination of their fate, which indirectly reflects the fate of their payload, making it particularly useful for evaluating the effectiveness of the delivery system *in vivo*.

Magnetic iron oxide nanoparticles (MNPs) have been widely used as a new type of magnetic resonance contrast agent for their excellent safety and biocompatibility profile.¹⁴ They have been used for multiple purposes such as detection of different diseases, including inflammatory and degenerative diseases, early tumor detections^{15,16} and blood-brain barrier transport.¹⁷ Recently, their potential as a drug delivery system has been brought under the spotlight. In the present study, we report the construction of a miRNA delivery probe using a well-defined poly(ethylene glycol) (PEG)-coated Fe₃O₄ nanoparticle (MNP) as both carrier and MRI contrast agent. The delivery efficiency and therapeutic effect of this particular magnetic nanoparticle-based miR16 carrier in drug resistant SGC7901 cells were assessed in both *in vitro* and *in vivo* models. Our results demonstrated that Fe₃O₄ nanoparticles conjugated with miR16 (miR16/MNPs) can effectively deliver miR16 to SGC7901/ADR cells and increase their sensitivity to adriamycin (ADR).

Materials and methods

Animals

Specific pathogen-free 8-week-old female Balb/c nude mice were obtained from the Shanghai Animal Center in China and bred in the Fourth Military Medical University animal center, China. All the experimental animals were housed under specific pathogen-free conditions. The animal protocols used in this study were approved by the Fourth Military Medical University Ethics. All the procedures were performed in accordance with the Fourth Military Medical University Guide for the Care and Use of Laboratory Animals formulated by the National Society for Medical Research.

Reagents and antibodies

MNPs were synthesized by a modified “one-pot” synthetic approach according to our previous reports.^{18,19} Cy5.5 NHS ester was purchased from GE (GE Healthcare, Piscataway, NJ, USA). The miR16 and negative control (NC) RNA oligos were synthesized (Shanghai GenePharma, China) using the following sequences: miR16 sense: 5'-UAGCAGCAGUAAAUAUUGGCG-3';

N.C. sense: 5'-UUGUACUACACAAAAGUACUG-3'. The anti-cancer drug ADR was purchased from Wolsen Biotechnology (Xi'an, China). Rabbit polyclonal antibody specific to Bcl-2 was purchased from Santa Cruz Biotechnology (Santa Cruz, CA). Antibody specific to human sodium iodide symporter (hNIS), cleaved form of caspase3 and poly (ADP-ribose) polymerase (PARP), as well as β -actin were purchased from Abcam (Cambridge, UK). The terminal deoxynucleotidyl transferase-mediated dUTP nick end-labeling (TUNEL) cell apoptosis detection kit was provided by Beyotime Institute of Biotechnology (Haimen, China). All cell culture media and serum were purchased from Gibco (Grand Island, NY).

Cell culture

Human gastric cancer cell line SGC7901 and its multidrug resistant (MDR) variant SGC7901/ADR were established and maintained in our laboratory as previously described. In brief, they were cultured in RPMI-1640 medium supplemented with 10% fetal calf serum and 100 units penicillin and 100 mg ml⁻¹ streptomycin (Invitrogen). To maintain the MDR phenotype, ADR with final concentration of 0.5 mg ml⁻¹ was added to the culture medium.

SGC7901/ADR^{fluc} and NF/3×miR16 SGC7901 were also established and cultured in our laboratory.²⁰ Fluc (firefly luciferase reporter) gene is encoded by SGC7901/ADR^{fluc} cell lines. Once the luminescent substrate D-luciferin is added, SGC7901/ADR^{fluc} can exhibit a bioluminescence signal that can be captured by a particular imaging system. As to NF/3×miR16 SGC7901, a dual expression vector was constructed by inserting the cDNA of hNIS gene into the BamH and Age I restriction enzyme sites of a lentiviral vector GV260-Fluc-puro (Shanghai GeneChem, China) that encoded Fluc. After that, the copies of complementary sequences against miR16 were inserted after the stop codon of the hNIS/Fluc gene. The constructed vector was used to infect SGC7901 cells, which resulted in the NF/3×miR16 SGC7901 cell line. In this cell line, fluc fluorescence intensity and hNIS expression are reversely correlated with the intracellular miR16 level and can be used as an indirect index of miR16 intracellularly.

Preparation of PEG-coated Fe₃O₄ nanoparticles (MNPs)

First, biocompatible Fe₃O₄ nanoparticles were synthesized as previously reported. Typically, 2.1 g of Fe(acac)₃ (6 mmol), 7.9 mL of oleylamine (24 mmol), and 24 g of amine terminated PEG (12 mmol) were dissolved in 100 mL of diphenyl ether solution. The solution was purged with nitrogen for 2 h to remove oxygen with mechanical stirring at 400 rpm. After being incubated at 80 °C for 4 h, the reaction mixture was quickly heated to reflux within 10 min and maintained at reflux for 30 min for monitoring particle formation and growth. Ether was introduced to precipitate and isolate the resultant Fe₃O₄ nanocrystals from the reaction mixture after it was cooled to room temperature. Then, the precipitate was re-dissolved in ethanol followed by the addition of ether as precipitant. Typically, this purifying procedure was repeated for three cycles. After that, the PEG-coated Fe₃O₄ nanoparticles

were purified and dissolved in either Milli-Q water or PBS for further experiments.

Preparation of Cy5.5-conjugated MNPs

Cy5.5 mono-NHS ester (2.25 mg), a commonly used fluorescent dye, dissolved in 250 μL of dimethyl sulfoxide (DMSO) was slowly added to 50 mg of MNPs, which was dispersed in 50 ml of PBS. After being allowed to react on ice in the dark with vigorous stirring for 24 h, unreacted Cy5.5 was removed by gel filtration on Sephadex G-50. After labeling, the mixture was dialyzed using an 8.0 kDa molecular weight cut-off membrane (Spectrum Chemicals & Laboratory Products, California, USA), followed by lyophilization. Finally, Cy5.5 was conjugated with the amino groups of PEG to allow the *in vivo* tracking of MNPs distribution by fluorescence imaging. These resulting Cy5.5-conjugated MNPs were stored at 4 $^{\circ}\text{C}$ in the dark for further use.

Synthesis of miR16/MNPs

miRNA (purchased from Jima, China) was negatively charged and the surfaces of MNPs were positively charged. Therefore, miRNA and MNPs can be linked by electrostatic interaction. In brief, miR16 was dissolved in Milli-Q water, and then mixed with MNPs at room temperature for 1 h. miR16/MNPs were characterized at 298.0 K *via* the dynamic light scattering (DLS) method using an instrument (Nano ZS, Malvern) equipped with a solid-state He-Ne laser ($\lambda = 633 \text{ nm}$). The efficacy of the miRNA linked to MNPs was evaluated by agarose gel

electrophoresis. The structure of ultimately synthesized miR16/MNPs conjugated with Cy5.5 was illustrated as Fig. 1A.

Characterization of miR16/MNPs

TEM (transmission electron microscopy) images were obtained using a transmission electron microscope (JEM-100CXII) operating at an accelerating voltage of 100 kV. More than 400 quasi-spherical particles were measured to obtain the average equivalent area and diameter of the MNPs. Magnetization measurements were obtained using a vibrating sample magnetometer (VSM JDM-13, China). The hydrodynamic size of the samples was characterized at 298.0 K by DLS using an instrument (Nano ZS, Malvern) equipped with a solid-state He-Ne laser ($\lambda = 633 \text{ nm}$). The organic content was measured by thermogravimetry analysis (TG/DTA 6300, SII Nanotechnology Inc). The efficacy of the miRNA linked to MNPs was evaluated by agarose gel electrophoresis.

Determination of cell toxicity of MNPs by MTT

20 000 Cells were plated into each well of 96-well flat-bottomed micro-titer plates. After 12 h incubation at 37 $^{\circ}\text{C}$, a medium containing MNPs ($0 \mu\text{g ml}^{-1}$ to $20 \mu\text{g ml}^{-1}$) was added to the cells. After 48 h incubation, 20 μl of 5 mg ml^{-1} MTT was introduced into each well and incubated for 4 h of exposure. The plates were centrifuged and medium was decanted. Subsequently, the cells were dissolved in 150 μl DMSO with gentle shaking for 10 min at room temperature followed by measurement of OD 490 nm. Eight replicate wells were used at each point in three separate measurements.

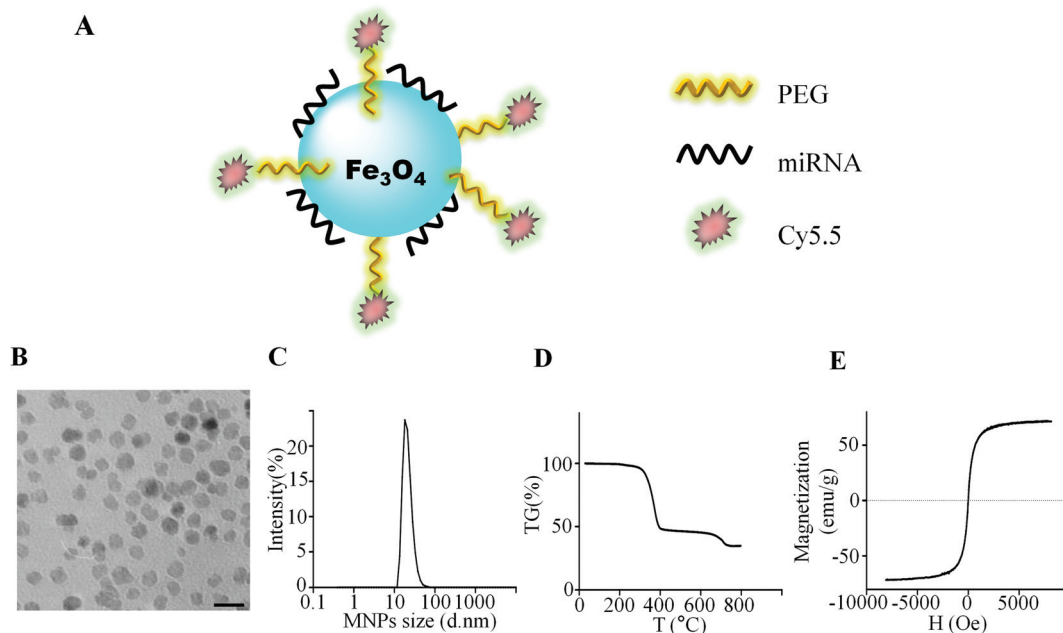


Fig. 1 (A) Schematic illustration of miR16/MNPs. (B) Morphological observations of MNPs. Scale bar = 50 nm. (C) Particle size distribution of MNPs. (D) The organic content of MNPs. (E) Magnetization of MNPs.

Evaluation of intracellular uptake of MNPs

Intracellular uptake of MNPs by SGC7901 cells after co-culture *in vitro* was examined by Prussian blue staining and ICP-AES analyses were performed as previously reported. In brief, after incubation with $10 \mu\text{g ml}^{-1}$ MNPs, 1×10^4 SGC7901 cells were washed with PBS and fixed for 15 min using 4% paraformaldehyde (Sigma-Aldrich). Then cells were washed with PBS and incubated with freshly prepared Pers' reagent (4% potassium ferrocyanide [Sigma-Aldrich]–12% HCl, 1:1, v/v) for 10 min. Then, the cells were washed three times with PBS. Tumor tissue was counterstained with neutral red (0.02%) (Sigma-Aldrich), and subsequently observed by an inverted optical microscope. ICP-AES was performed to quantify Fe to detect the dose of MNPs in the SGC7901 cells. After incubation with MNPs at 1, 2, 3, 5 h, cells were washed with PBS, and then dissolved in sulfuric acid and nitric acid. Then, the concentration of Fe was measured by ICP-AES.

In vitro cells apoptosis assay

5×10^5 SGC7901/ADR cells per well were seeded in 6-well plates. 24 h after co-culture with 100 nM miR16/MNPs (200 pmol miR16 loaded by $16.6 \mu\text{g}$ MNPs in 2 ml medium), cells were collected and drug sensitivity of which was evaluated by TUNEL and FACS. The SGC7901/ADR cells treated as aforementioned were fixed with 4% paraformaldehyde, rinsed with PBS, and then permeabilized by 0.1% Triton X-100 for FITC end-labeling the fragmented DNA of the apoptotic cells using TUNEL cell apoptosis detection kit. The FITC-labeled TUNEL-positive cells were imaged under fluorescent microscopy using 488 nm excitation and 530 nm emission. For FACS assay, after 100 nM miR16/MNPs were co-cultured with 5×10^5 SGC7901/ADR cells for 24 h and the cells were incubated with anti-cancer drugs ADR for 48 h. Then, the cells were harvested, and the Annexin V-FITC Apoptosis Detection Kit (BD Biosciences) was used for apoptosis assays. Cells were stained according to the manufacturer's protocol and sorted using a FACS sorter (BD Biosciences, La Jolla, CA, USA), and the data were analyzed using ModFit software (BD Biosciences).

In vitro bioluminescence imaging

NF/3×miR16/SGC7901 cells were constructed as described in our previous report.²⁰ Before nanoparticle treatment, NF/3×miR16/SGC7901 cells were seeded at 1×10^4 cells per well in a 24 well plate. After 24 h, miR16/MNPs and N.C./MNPs were co-cultured with NF/3×miR16/SGC7901 cells. The concentration of miR16/MNPs or N.C./MNPs is from low to high (0 nM, 25 nM, 50 nM, 75 nM and 100 nM). Typically, every 60 pmol miR16 was loaded with $5 \mu\text{g}$ MNPs. After 72 h, each well was washed with PBS. Then, D-luciferin (Xenogen Corporation, Massachusetts, USA) (0.5 mmol L^{-1}) was immediately added before assay. Bioluminescence signal was captured with an IVIS 100 Imaging system (Xenogen Corporation, Massachusetts, USA) and the intensity was analyzed using the Living Image software version 2.50.

Experimental protocol *in vivo*

SGC7901/ADR^{fluc} (5×10^6) were subcutaneously xenografted into the right shoulder of each female nude mouse age 6–8 weeks ($n = 18$). When the diameter of tumor reached around 0.5 cm, mice were randomly divided into 3 groups: group I (saline), group II (N.C./MNPs) and group III (miR16/MNPs). Saline, N.C./MNPs (5 mg kg^{-1}) or miR16/MNPs (5 mg kg^{-1}) loading 1.0 nmol miR16 was intravenously injected *via* tail vein at day0, day3, day7, day10, day14, day17 and day21 post establishment of xenografted tumor model. ADR (2.5 mg kg^{-1}) was administered at day0, day7, day14 and day21 by intraperitoneal injection. Tumor volume ($V = AB^2/2$, where A is the tumor length and B is the tumor width) was calculated and BLI was obtained every week.

Bioluminescent imaging (BLI), fluorescent imaging (FI) and magnetic resonance imaging (MRI) of nude mice *in vivo*

After establishment of SGC7901/ADR^{fluc} xenografted tumor model, BLI was performed using the IVIS 100 system in a serial of time points (day7, day14, day21 and day28) post nanoparticles injection. Bioluminescence signal was captured 5 min after the intravenous injection of D-luciferin (0.5 mmol L^{-1}) into mice under anesthesia by isoflurane. Bioluminescence and Cy5.5 fluorescence signals were detected using the IVIS 100 system.

MRI was analyzed by a 3-T MRI system (Siemens, Germany). In brief, the tumor-bearing mice were intravenously injected with MNPs (5 mg kg^{-1}); before and after injection for 24 h, MR imaging was conducted on a 3-T clinical MRI scanner.

Statistical analysis

Results are expressed as mean \pm standard deviation (SD). SPSS17.0 (SPSS Inc., USA) and Prism 5.0 (GraphPad Software, USA) were used to perform the one-way analysis of variance (ANOVA). A two-tailed P -value <0.05 was considered significant.

Results

Characterization of MNPs

MNPs were synthesized by thermal decomposition. A representative transmission electron microscopy (TEM) image of the resulting biocompatible Fe_3O_4 nanoparticles is shown in Fig. 1B, with a size range from $12.4 \pm 1.6 \text{ nm}$. Fig. 1C reveals that the average hydrodynamic size of the MNPs is about 48.6 nm. The organic content of the current MNP sample was around 65.3% (Fig. 1D). Fe_3O_4 nanocrystals are superparamagnetic and present a saturation magnetization of 63.5 emu g^{-1} at $25 \text{ }^\circ\text{C}$ (Fig. 1E).

Cytotoxicity assay of MNPs

Cell viability studies were performed by incubating MNPs with SGC7901 cells at different concentrations and assaying the cell metabolic activity after 24 h. Fig. 2A showed the low toxicity of MNPs even at the highest concentration of $20 \mu\text{g ml}^{-1}$. The

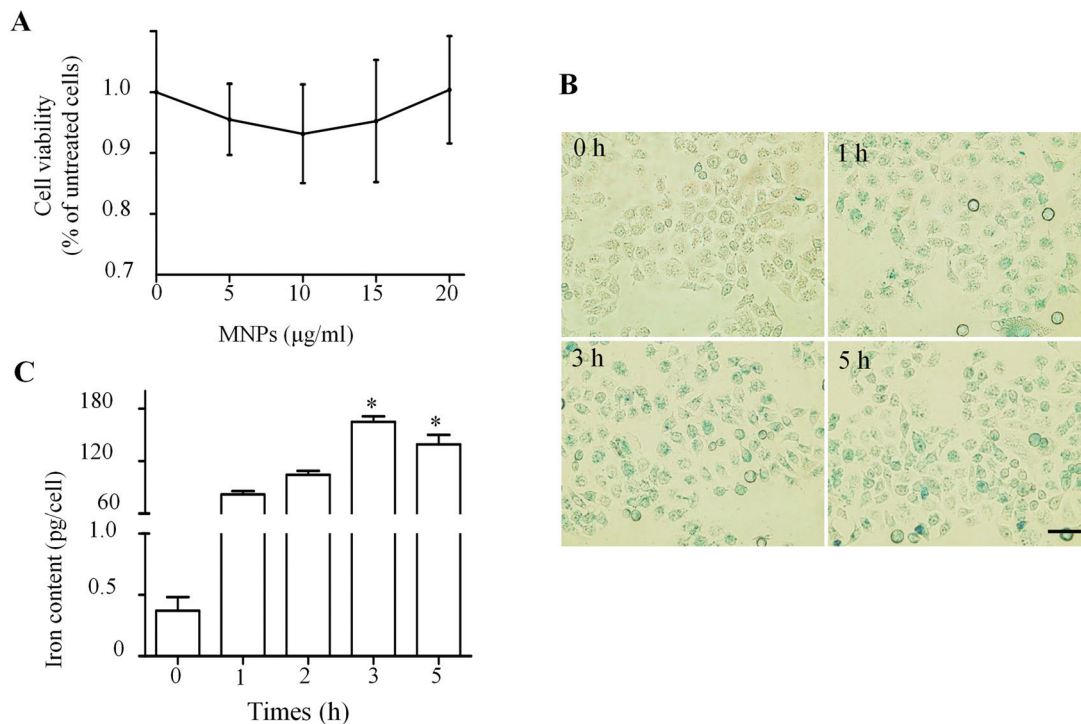


Fig. 2 (A) Cytotoxicity of MNPs to SGC7901 cells by MTT assay. (B) Microscope images of Prussian blue dye stained SGC7901 cells. The iron in the cells was stained blue. (C) Fe-iron accumulation in SGC7901 cells detected by ICP AES analysis. * $P < 0.05$ compared at 2 h.

excellent biocompatibility of the MNPs may be attributed to the introduction of biocompatible PEG into the MNPs.

Intracellular uptake of MNPs

Prussian blue staining and ICP-AES analyses were conducted to determine the fate of MNPs after incubation with SGC7901 cells *in vitro* and showed that MNPs began to enter cells after 1 h of co-culture and reached the peak at 3 h (Fig. 2B and C). The concentration of iron per cell modestly decreased at 5 h, which may be due to exocytosis.

Characterization of miR16/MNPs

TEM was used to assess the size of miR16/MNPs. After MNPs (10 µg) coupled with 10, 20, 30 and 40 pmol miR16, the produced miR16/MNPs did not show significant variation in size (Fig. 3A and B). The reasonable increase of the hydrodynamic size strongly suggested that miR16 was effectively loaded onto the MNPs *via* electrostatic interaction. Zeta-potential of MNPs was measured as a range of 6.65 ± 0.78 mV, while changing to -7.6 ± 0.21 mV after coupling with miR16 (Fig. 3C). To determine the stability of miR16/MNPs, we measured the hydrodynamic size of miR16/MNPs at 0 h, 12 h, 24 h and 48 h. Results showed miR16/MNPs remained stable at 48 h (Fig. 3D). In addition, we examined miRNA binding ability using agarose gel electrophoresis. MNPs were mixed with miR16 at various weight ratios, and then incubated for 60 min to form polyelectrolyte complexes. As Fig. 3E shows, the content of free miRNA gradually decreased with increasing weight ratio indicating the successful formation of charge-neutralized polyelectrolyte com-

plexes. In addition, Fig. S2A† shows images of miR16/MNPs in various media such as PBS, saline, cell medium and serum, which revealed good water solubility and stability of miR16/MNPs. After the centrifugation filtration, no noticeable miRNA was detected in the removed solution by agarose gel electrophoresis analysis (Fig. S2B†), indicating sound conjugation of miR16 with MNPs without significant detachment even in serum.

miR16/MNPs increased the functional expression of miR16 in SGC7901 cells

NE/3×miR16 SGC7901 cells were employed to assess the expression of miR16 in SGC7901 cells post transfection. After being co-cultured with miR16/MNPs, SGC7901 cells dramatically exhibited decreased luminescence intensity, compared with N.C./MNPs treatment (Fig. 4A and B), indicating that miR16/MNPs are able to increase the expression of miR16 in NE/3×miR16 SGC7901 cells, which was also confirmed by the reduction of hNIS expression (Fig. 4C and D). Then, we detected the expression of Bcl-2, the endogenous target gene of miR16, which was significantly reduced in the miR16/MNPs group (Fig. 4E and F). These combined results indicate the successful intracellular introduction of miR16/MNPs and this introduction might increase the functional level of miR16 in targeted cells.

miR16/MNPs increased the sensitivity of SGC7901/ADR cells to ADR *in vitro*

TUNEL, MTT and FACS assay were performed to assess the sensitivity of SGC7901/ADR cells to ADR after being treated

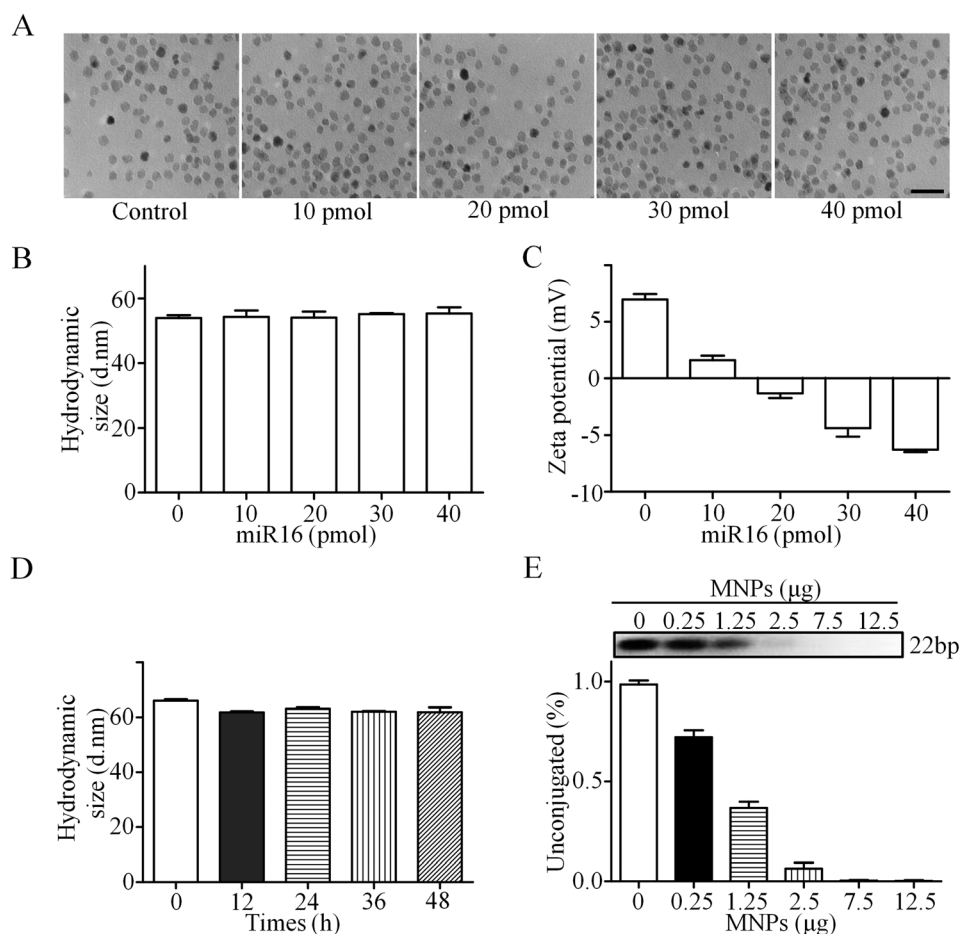


Fig. 3 (A) Morphological observations of miRNA/MNPs. Scale bar = 50 nm. (B) and (C) After 10 μg MNPs were connected to 0, 10, 20, 30 and 40 pmol miRNA, the hydrodynamic size (B) and Z-potential (C) of the samples were characterized at 298.0 K by a DLS using an instrument. (D) The hydrodynamic size of miRNA/MNPs was characterized at 0, 12, 24, 36 and 48 hours. (E) Agarose gel electrophoresis for analysis of unconjugated miR16/MNPs ratio. Lane 1: 60 pmol miR16; Lane 2: 60 pmol miR16 and 0.25 μg MNPs; Lane 3: 60 pmol miR16 and 1.25 μg MNPs; Lane 4: 60 pmol miR16 and 2.5 μg MNPs; Lane 5: 60 pmol miR16 and 7.5 μg MNPs; Lane 6: 60 pmol miR16 and 12.5 μg MNPs.

with miR16/MNPs or N.C./MNPs for 24 h. TUNEL staining showed that, after co-culture with nanoparticles, the miR16/MNPs group showed higher apoptotic rate (24.8%) than both the N.C./MNPs treated group (14.5%) and the control group (12.4%) (Fig. 5A and B). MTT test demonstrated that the IC_{50} of ADR in miR16/MNPs treated cells is 2.0 mg ml^{-1} , which is significantly lower than that of control or N.C./MNPs treated cells (Fig. 5C). FACS assay also showed considerably more apoptotic cells in the miR16/MNPs group than the other two groups (Fig. 5D). Furthermore, we examined the effect of miR16/MNPs on caspase3 activation by Western blot analysis. As shown in Fig. 5E, the treatment of SGC7901 cells with miR16/MNPs led to drastic activation of caspase3, as evidenced by increased cleaved-caspase3 level (Fig. 5F). We also detected the effect of miR16/MNPs on the death substrate poly (ADP-ribose) polymerase (PARP), which is capable of mediating DNA fragmentation during apoptosis upon switching from pro- to active forms by cleaved caspase3. Our results revealed that the activation of caspase3 correlated with activation and cleavage of PARP (Fig. 5G). All these data suggested that

miR16/MNPs could sensitize SGC7901/ADR cells to ADR-induced apoptosis.

miR16/MNPs accumulated passively in tumor area *in vivo*

An IVIS 100 Imaging system and a 3-T MRI system were employed to obtain optical imaging signal and MRI signal, respectively. MNPs were labeled with Cy5.5 NHS ester for *in vivo* imaging. Before injection, successful Cy5.5/MNPs connection was confirmed by N-IR (near infra-red) optical imaging. As can be seen from Fig. 6A and 6B, similar fluorescence intensity was produced by Cy5.5 and Cy5.5/MNPs, while no signals were generated by unmodified MNPs. The tumor uptake of Cy5.5/MNPs was detected by N-IR optical imaging and MRI *in vivo*, as well as Prussian blue staining *ex vivo*. Both MRI (left panel) and fluorescent imaging (middle panel) modalities showed the enrichment of MNPs in the tumor site (Fig. 6C), which was also confirmed by Prussian blue staining (Fig. 6D). These data indicated miR16/MNPs were able to achieve targeted accumulation in the tumor site after systemic administration, which might be attributed to EPR effect. Moreover, the

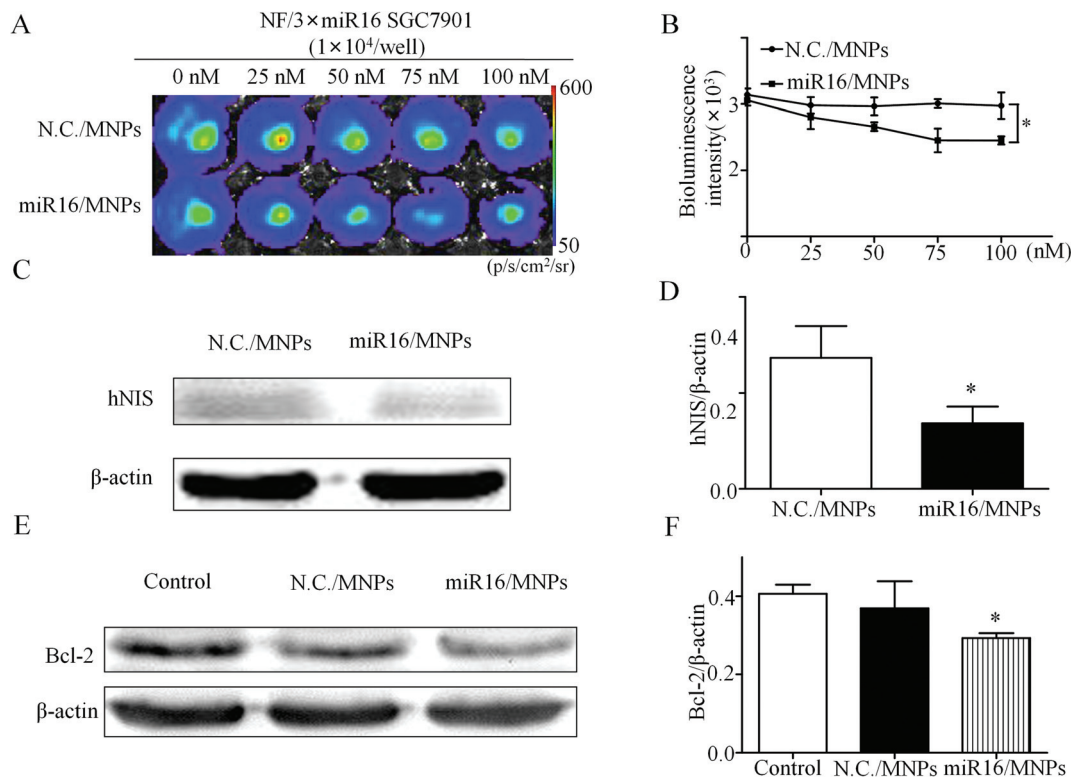


Fig. 4 (A) Representative bioluminescence images of NF/3xmiR16 SGC7901 cells treated by miR16/MNPs or N.C./MNPs (N.C. means negative control miRNA) *in vitro*. (B) Statistical analysis of BLI signals intensity in different groups. Representative Western blot images (C) and semiquantification (D) of hNIS expression after NF/3xmiR16 SGC7901 cells treated by miR16/MNPs or N.C./MNPs. Representative Western blot images (E) and semiquantification (F) of Bcl-2 expression after NF/3xmiR16 SGC7901 cells treated by miR16/MNPs or N.C./MNPs. * $P < 0.05$ compared with N.C./MNPs group.

BLI imaging confirmed the successful establishment of SGC7901/ADR^{fluc} tumor with the overexpression of the fluc gene, which can generate a strong bioluminescence signal (right panel; Fig. 3C). Moreover, to evaluate the toxicity of our synthesized miR16/MNPs *in vivo*, we harvested the major organs of miR16/MNPs treated mice for histology analysis, including heart, liver, spleen and kidney. Compared with normal tissue, no noticeable damage of those critical organs was observed from H&E staining (Fig. S1†), indicating the feasibility of systemic use of miR16/MNPs.

miR16/MNPs increased the sensitivity of SGC7901/ADR cells to ADR *in vivo*

Mice bearing tumor were injected with ADR (2.5 mg kg⁻¹, IP) twice a week by intraperitoneal injection. miRNA/MNPs containing 1 nmol miRNA or equivalent amount of N.C./MNPs were injected once every week *via* tail vein. Tumor bioluminescence imaging and tumor volume measurement were performed every week. As shown in Fig. 7A and 7B, the bioluminescence signal intensity of tumor decreased over time in the miR16/MNPs group, whereas it increased in the control or N.C./MNPs groups. At day 28, compared to control or N.C./MNPs group, the luciferase signal in miR16/MNPs group was significantly lower indicating the death of tumor cells and

reduction of tumor size post miR16/MNPs administration. Tumor volume measurement also confirmed tumor size reduction in miR16/MNPs group (Fig. 7C). Moreover, we also collected the tumor slice to further confirm the effect of systemic use of miR16/MNPs on cancer cell apoptosis by TUNEL staining. As Fig. S4† shows, the amount of apoptotic nuclei remarkably increased within cancer tissue after miR16/MNPs administration, indicating the induced apoptosis of cancer cells *in vivo* by miR16/MNPs. Taken together, our results indicated that miR16/MNPs increased the sensitivity of SGC7901/ADR cells to ADR *in vivo*.

Discussion

Drug resistance is one of the most common causes of chemotherapy failure in the treatment of gastric cancer. Multi-drug resistance (MDR) in cancer refers to the capacity of cancer cells to survive or become resistant to treatment with a wide variety of anti-tumor medications. The mechanisms of MDR include a decreased uptake of drugs, reduced intracellular drug concentration by the activation of the efflux transporters, modifications in cellular pathways by altering cell cycle checkpoints, increased metabolism of drugs, induced

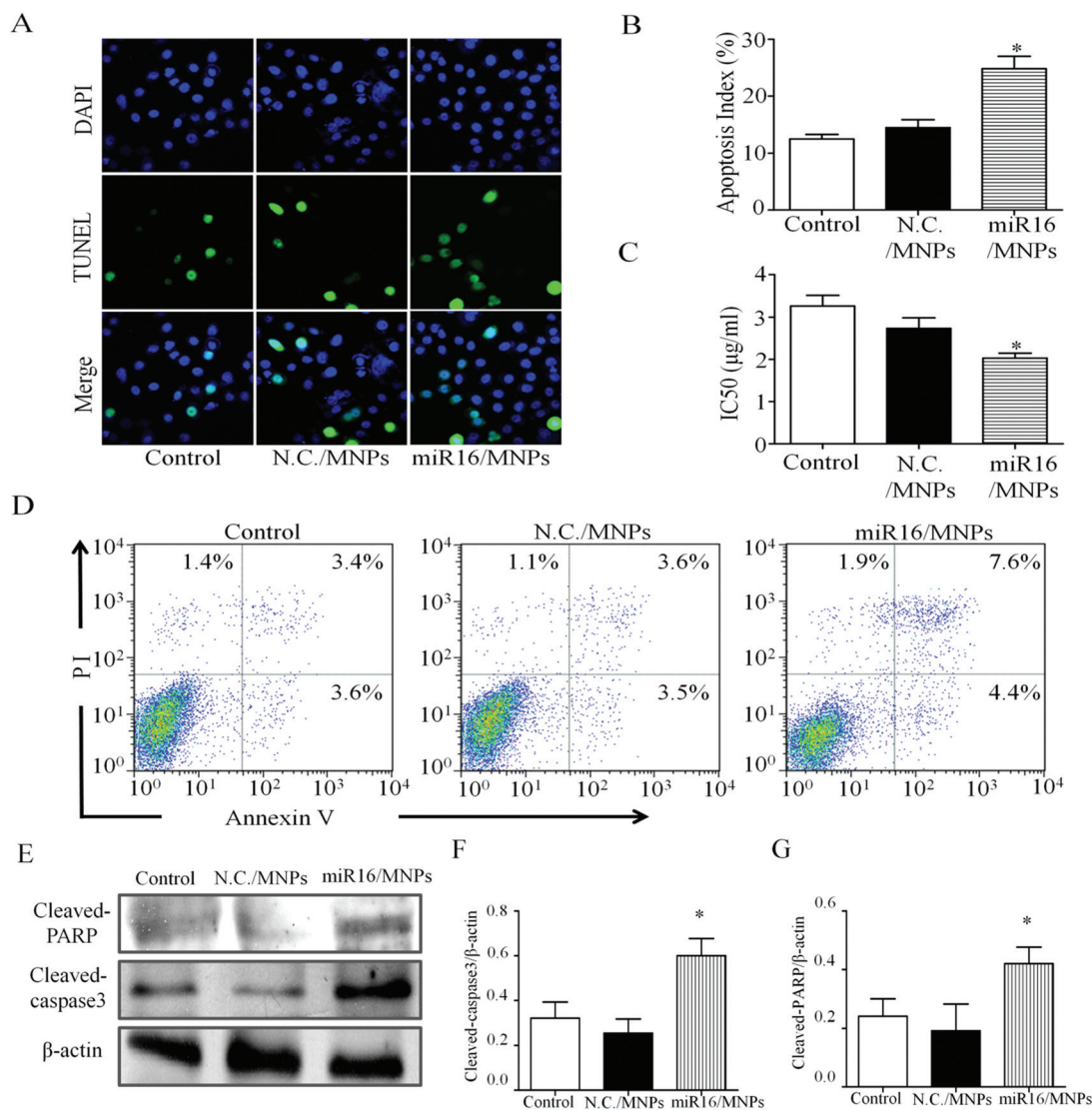


Fig. 5 (A) and (B) Apoptotic cells were detected by TUNEL staining. (C) IC₅₀ of ADR in SGC7901/ADR cell lines after treatment with N.C./MNPs or miRNA/MNPs. (D) Apoptotic cells were detected by FACS assay. Representative Western blot images (E) and semiquantification of cleaved-caspase3 expression (F) and cleaved-PARP expression (G) after NF/3XmiR16 SGC7901 cells treated by miR16/MNPs or N.C./MNPs. **P* < 0.05 compared with **P* < 0.05 compared with N.C./MNPs group.

emergency response genes to impair apoptotic pathways and altered DNA repair mechanisms. Despite the discovery of multiple new gene/protein expression signatures or factors associated with drug resistance by high throughput “-omics” technologies, little clinical success has been obtained in reversing MDR *via* traditional strategies such as the development of ATP-binding cassette transporter inhibitors.²¹

It has been reported that changes in miRNA expressions were involved in drug resistance and the modulation of miRNA expression could partially overcome drug resistance and pronouncedly improve the anti-tumor activity of certain drugs.²² To date, many miRNAs are found involved in the drug resistance of gastric cancer.³ In our previous work, the overexpression of miR15b or miR16 could sensitize SGC7901/VCR cells to anticancer drugs by targeting Bcl-2 in human gastric cancer

cells. Moreover, the overexpression of miR15b or miR16 could sensitize SGC7901/VCR cells to VCR-induced apoptosis. Proving that, in theory, it is possible to reverse MDR in gastric cancer cells.⁶ However, the manipulation of miR16 expression *via* a viral delivery system is hampered by safety concerns as to its clinical application.

In the past few years, nanoparticles have been emerging as particularly promising gene therapy vectors. Because of their controlled release characteristics and biocompatibility, nanoparticles conjugated with miRNA could release their payload over extended periods of time making them potential candidates for miRNA delivery to MDR cancer tissue. Traditional nanoprobe for miRNA imaging and delivery have several drawbacks, including sophisticated synthetic processes, limited intensity for detection *in vivo*, low efficacy upon

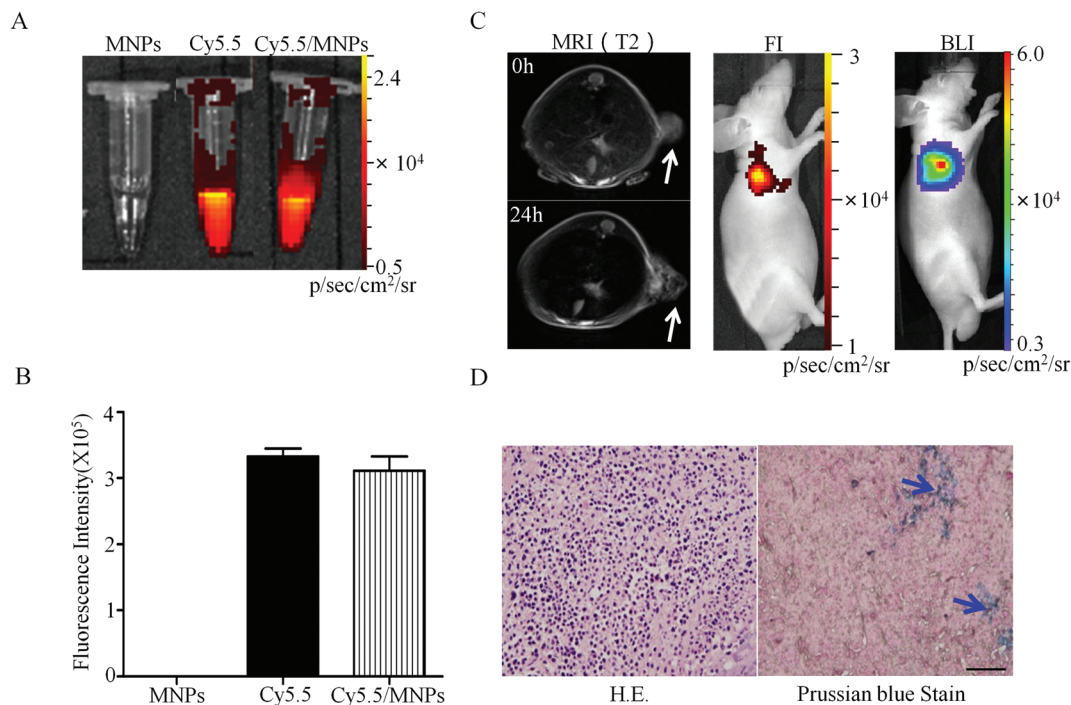


Fig. 6 (A) Representative fluorescence images of MNPs, Cy5.5 and Cy5.5/MNPs. (B) Statistical analysis of fluorescence signal intensity in different groups. (A) and (B) Fluorescence imaging of MNPs, Cy5.5 and Cy5.5/MNPs. (C) Distribution of Cy5.5/MNPs after injection was detected by MRI, bioluminescence imaging and fluorescence imaging. (D) H&E and Prussian blue staining of cancer tissue. Magnification 40x; scale bar = 500 μ m.

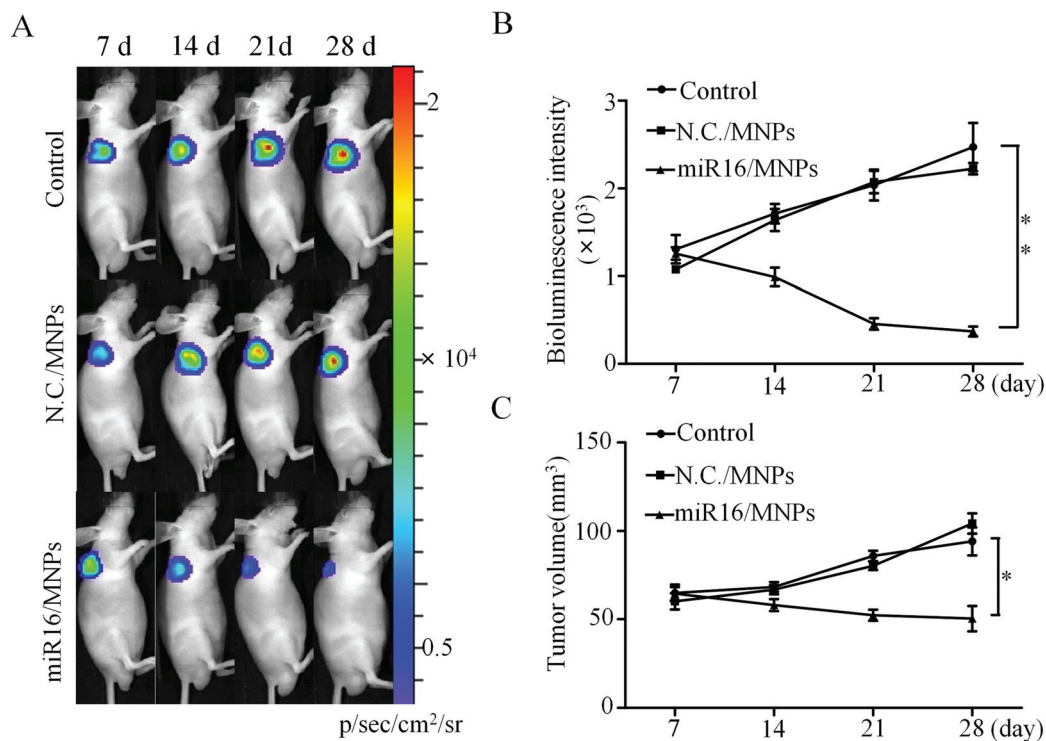


Fig. 7 (A) Representative bioluminescence images of SGC7901/ADR^{fluc} tumor in a series of time points (day7, day14, day21 and day28) after treatment with miR16/MNPs or N.C./MNPs *in vivo*. (B) Statistical analysis of BLI signals intensity in different groups. (C) Tumor volume measurement of different groups in a series of time points (day7, day14, day21 and day28). $N = 6$, * $p < 0.05$ compared with the control group.

systemic administration and potential toxicity to normal tissue.^{23,24} The PEG-coated Fe₃O₄ nanoparticle carrying miR16 (miR16/MNPs), which we synthesized here exhibited its own superiorities. First, we employed the thermal decomposition method to develop a simple route for synthesizing water-soluble and biocompatible magnetic nanoparticles with PEG modification *via* a “one-pot” reaction.¹⁵ Second, the surface modification of nanoparticles with PEG prolongs blood half-life and enhances the bioavailability of miR16/MNPs, owing to the increased retention of the complex in serum without affecting the silencing ability of miRNA portion.^{25,26} Prolonged silencing *in vivo* by PEGylated reagent could lower the doses required for effective therapy, reducing dosage-dependent adverse effects. Moreover, the main component of MNPs is iron oxide, which is biodegradable and bears minimal toxicity.²⁷ Third, relatively large Fe₃O₄ nanoparticles led to strong MR contrast enhancement effect without compromising the loading capacities for both miR16 and dye Cy5.5, resulting in a strong silencing ability as well as a decent fluorescence imaging signal. Finally, it has been well-documented that nanoparticles can be targeted to tumors with high vascular permeability through EPR (enhanced permeability and retention) effect, achieving higher drug concentration at the target site. This effect can markedly increase the local concentration of miR16/MNPs and improve the efficacy of miR16 delivery.

In our study, miR16/MNPs accumulation in tumor was demonstrated by both *in vivo* and *in vitro* examination. The delivery efficiency was first evaluated by bioluminescence intensity measurement *in vitro*. In cultured NF/3×miR16 SGC7901 cells, miR16/MNPs treatment significantly reduced the intensity of bioluminescence, suggesting the successful introduction of miR16. The introduction of miR16 was further confirmed by down-regulation of Bcl-2, target gene of miR16 as discovered in our previous study. Targeting of the miRNA payload to the tumor *in vivo* is vital for the success of nanoparticle based therapy. We injected miR16/MNPs into mice with SGC7901/ADR^{fluc} cells subcutaneously xenografted. The advent of molecular imaging techniques noninvasively allows the visualization of many pathophysiological processes in living subjects at the molecular level. Nanoparticles could be traced *in vivo* by molecular imaging *via* their intrinsic character or by fluorescent dye and radioactive isotope attached to the particles.^{28,29} In this research, we took advantage of the magnetic property of iron oxide core and conjugated fluorescent dye on the surface of nanoparticles to simultaneously obtain both MR imaging and optical imaging *in vivo*. The accumulation of miR16/MNPs in the tumor area was evidenced by a strong fluorescence signal generated by Cy5.5 linked on the surface and MRI signal generated by the magnetic Fe₃O₄ core.

In addition to dissatisfying treatment outcome, the traditional approach often leads to the inaccurate evaluation of disease progression and therapeutic effect for the lack of an ideal monitoring tool. Consequently, combining functional molecular imaging with elaborately designed nanoparticles is of great importance and facilitates the advancement of cancer diagnosis and therapy because of the advantages of favorable

pharmacodynamics, target specificity and quantitative nature.³⁰ In our study, multifunctional Fe₃O₄ nanoparticles loaded with miR16 produced a remarkable effect on sensitizing SGC7901 cells to ADR. However, some previous studies reported that magnetic iron oxide nanoparticles were able to induce drug sensitivity especially to another ADR-class drug, doxorubicin (DOX) in a magnetic field.³¹ This phenomenon could be attributed to increased DOX release and/or the hyperthermia effect of a high frequency magnetic field.³² To exclude the possible effect caused by magnetic field, we employed MNPs without loading miR16 as the negative control in our work and our data demonstrated that MNPs alone did not lead to a noticeable effect on sensitizing SGC7901 cells to ADR, compared with blank control. However, we think it would be very interesting to investigate in our future work whether MNP plays a synergistic role with miR16. In addition, EPR effect and PEG modification of miR16/MNPs guaranteed good biocompatibility and favorable therapeutic effect *in vivo*, which was supported by reduced tumor volume, as well as decreased bioluminescence signal in tumor area dynamically monitored by BLI imaging. Furthermore, we linked Cy5.5 to MNPs, which has the potential to allow *in vivo* tracking by both MRI and fluorescent imaging at the same time; thus, the comprehensive theranostic evaluation of the gastric cancer might be obtained.

Although our results showed significant suppression of tumor growth, more effort is required to further understand the *in vivo* behaviors and improve both diagnostic and therapeutic efficacy of miRNA-loaded MNPs, including the determination of proper dose and duration of particles delivery using a larger cohort of animals, the synthesis of new nanoparticles conjugated with specific antibody in order to achieve active targeting; and selecting other potent miRNAs to obtain better effect of cancer therapy.

In summary, we developed and characterized a new MNP-based carrier for tumor-targeted delivery of miR16 in tumor-bearing mice, which can be well tolerated with a little toxicity. Our results showed the successful delivery of miRNA to the tumor tissue using MNPs both *in vitro* and *in vivo*, which was confirmed by multiple imaging modalities including fluorescence, MRI and bioluminescence imaging. Moreover, miR16/MNPs hold great potential for increasing the sensitivity of gastric cancer cells to ADR, the process of which could be dynamically monitored and accurately evaluated by a molecular imaging approach. Our work suggests the great promise of using miR16/MNPs in therapeutic application for treating drug-resistant gastric cancer.

Acknowledgements

This work was supported by National Nature Science Foundation of China (no.81090274, no.81270168, no.81325009, no.81227901 and no.81400366), Innovation Team Development Grant by China Department of Education (IRT1053), National Basic Research Program of China (2012CB518101).

References

- 1 D. Zhang and D. Fan, *Future Oncol.*, 2010, **6**, 527–537.
- 2 R. Wong and D. Cunningham, *Ann. Oncol.*, 2009, **20**, 605–608.
- 3 L. Hong, Z. Yang, J. Ma and D. Fan, *Curr. Drug Targets*, 2013, **14**, 1118–1127.
- 4 Q. Ma, X. Wang, Z. Li, B. Li, F. Ma, L. Peng, Y. Zhang, A. Xu and B. Jiang, *Oncol. Rep.*, 2013, **29**, 1652–1658.
- 5 M. Hao, L. Zhang, G. An, W. Sui, Z. Yu, D. Zou, Y. Xu, H. Chang and L. Qiu, *J. Hematol. Oncol.*, 2011, **4**, 37.
- 6 L. Xia, D. Zhang, R. Du, Y. Pan, L. Zhao, S. Sun, L. Hong, J. Liu and D. Fan, *Int. J. Cancer*, 2008, **123**, 372–379.
- 7 T. Behnke, J. E. Mathejczyk, R. Brehm, C. Wurth, F. R. Gomes, C. Dullin, J. Napp, F. Alves and U. Resch-Genger, *Biomaterials*, 2013, **34**, 160–170.
- 8 S. Cui, D. Yin, Y. Chen, Y. Di, H. Chen, Y. Ma, S. Achilefu and Y. Gu, *ACS Nano*, 2013, **7**, 676–688.
- 9 C. H. Fan, C. Y. Ting, H. J. Lin, C. H. Wang, H. L. Liu, T. C. Yen and C. K. Yeh, *Biomaterials*, 2013, **34**, 3706–3715.
- 10 H. Maeda, H. Nakamura and J. Fang, *Adv. Drug Delivery Rev.*, 2013, **65**, 71–79.
- 11 Y. Zhang, L. Peng, R. J. Mumper and L. Huang, *Biomaterials*, 2013, **34**, 8459–8468.
- 12 R. Shrestha, M. Elsabahy, S. Florez-Malaver, S. Samarajeewa and K. L. Wooley, *Biomaterials*, 2012, **33**, 8557–8568.
- 13 K. A. Whitehead, J. Matthews, P. H. Chang, F. Niroui, J. R. Dorkin, M. Severgnini and D. G. Anderson, *ACS Nano*, 2012, **6**, 6922–6929.
- 14 H. C. Huang, S. Barua, G. Sharma, S. K. Dey and K. Rege, *J. Controlled Release*, 2011, **155**, 344–357.
- 15 G. Yu, J. Li, W. Yu, C. Han, Z. Mao, C. Gao and F. Huang, *Adv. Mater.*, 2013, **25**, 6373–6379.
- 16 J. Chen, M. Shi, P. Liu, A. Ko, W. Zhong, W. Liao and M. M. Xing, *Biomaterials*, 2014, **35**, 1240–1248.
- 17 R. Qiao, Q. Jia, S. Huwel, R. Xia, T. Liu, F. Gao, H. J. Galla and M. Gao, *ACS Nano*, 2012, **6**, 3304–3310.
- 18 Q. Jia, J. Zeng, R. Qiao, L. Jing, L. Peng, F. Gu and M. Gao, *J. Am. Chem. Soc.*, 2011, **133**, 19512–19523.
- 19 S. Liu, Y. Han, R. Qiao, J. Zeng, Q. Jia, Y. Wang and M. Gao, *J. Phys. Chem. C*, 2010, **114**, 21270–21276.
- 20 F. Wang, X. Song, X. Li, J. Xin, S. Wang, W. Yang, J. Wang, K. Wu, X. Chen, J. Liang, J. Tian and F. Cao, *PLoS One*, 2013, **8**, e61792.
- 21 H. Lage, *Cell. Mol. Life Sci.*, 2008, **65**, 3145–3167.
- 22 S. Husted, R. Sokilde, L. Rask, S. Cirera, P. K. Busk, J. Eriksen and T. Litman, *Mol. Pharmacol.*, 2011, **8**, 2055–2062.
- 23 H. C. Huang, S. Barua, G. Sharma, S. K. Dey and K. Rege, *J. Controlled Release*, 2011, **155**, 344–357.
- 24 H. Song, R. He, K. Wang, J. Ruan, C. Bao, N. Li, J. Ji and D. Cui, *Biomaterials*, 2010, **31**, 2302–2312.
- 25 Q. Jia, J. Zeng, R. Qiao, L. Jing, L. Peng, F. Gu and M. Gao, *J. Am. Chem. Soc.*, 2011, **133**, 19512–19523.
- 26 S. M. Moghimi, A. C. Hunter and J. C. Murray, *Pharmacol. Rev.*, 2001, **53**, 283–318.
- 27 S. Laurent and M. Mahmoudi, *Int. J. Mol. Epidemiol. Genet.*, 2011, **2**, 367–390.
- 28 P. Chandrasekharan, D. Maity, C. X. Yong, K. H. Chuang, J. Ding and S. S. Feng, *Biomaterials*, 2011, **32**, 5663–5672.
- 29 J. Gao, K. Chen, R. Luong, D. M. Bouley, H. Mao, T. Qiao, S. S. Gambhir and Z. Cheng, *Nano Lett.*, 2012, **12**, 281–286.
- 30 F. F. Teng, X. Meng, X. D. Sun and J. M. Yu, *Int. J. Nanomed.*, 2013, **8**, 3703–3713.
- 31 H. Oliveira, E. Perez-Andres, J. Thevenot, O. Sandre, E. Berra and S. Lecommandoux, *J. Controlled Release*, 2013, **169**, 165–170.
- 32 M. Rahimi, S. Kilaru, G. E. Sleiman, A. Saleh, D. Rudkevich and K. Nguyen, *J. Biomed. Nanotechnol.*, 2008, **4**, 482–490.